JCB Journal of Cell Biology

ARTICLE

Mitotic phosphorylation of Pex14p regulates peroxisomal import machinery

Koichiro Yamashita[1*], Shigehiko Tamura[2*], Masanori Honsho[3,4], Hiroto Yada[1], Yuichi Yagita[3], Hidetaka Kosako[5], and Yukio Fujiki[3,4]

Peroxisomal matrix proteins are imported into peroxisomes via membrane-bound docking/translocation machinery. One central component of this machinery is Pex14p, a peroxisomal membrane protein involved in the docking of Pex5p, the receptor for peroxisome targeting signal type 1 (PTS1). Studies in several yeast species have shown that Pex14p is phosphorylated in vivo, whereas no function has been assigned to Pex14p phosphorylation in yeast and mammalian cells. Here, we investigated peroxisomal protein import and its dynamics in mitotic mammalian cells. In mitotically arrested cells, Pex14p is phosphorylated at Ser-232, resulting in a lower import efficiency of catalase, but not the majority of proteins including canonical PTS1 proteins. Conformational change induced by the mitotic phosphorylation of Pex14p more likely increases homomeric interacting affinity and suppresses topological change of its N-terminal part, thereby giving rise to the retardation of Pex5p export in mitotic cells. Taken together, these data show that mitotic phosphorylation of Pex14p and consequent suppression of catalase import are a mechanism of protecting DNA upon nuclear envelope breakdown at mitosis.

Introduction

Peroxisomes are ubiquitous, single-membrane-bounded organelles with a large variety of metabolic functions, such as β-oxidation of very-long-chain fatty acids and biosynthesis of plasmalogens (Fujiki, 1997; Lazarow and Moser, 1995). The peroxisome's metabolism depends on the import of nuclear gene-encoded proteins from the cytosol into each peroxisome (Lazarow and Fujiki, 1985). The majority of matrix proteins are destined for import into the peroxisomal matrix by a distinct dynamic system involving peroxins such as Pex1p, Pex2p, Pex5p, Pex6p, Pex7p, Pex10p, Pex12p, Pex13p, Pex14p, and Pex26p (Fujiki et al., 2006; Platta and Erdmann, 2007). The matrix proteins harbor the peroxisomal targeting tripeptide signal 1 (PTS1) at the C terminus or cleavable nonapeptide presequence PTS2 at the N terminus (Fujiki, 1997). These targeting signals are specifically recognized by the PTS1 receptor, Pex5p, and the PTS2 receptor, Pex7p (Fodor et al., 2015; Gatto et al., 2000; Otera et al., 2000, 2002). The soluble receptor–cargo protein complexes dock with Pex14p, the membrane peroxin of peroxisomal matrix protein importomer (Dias et al., 2017). After releasing the cargo into the peroxisomal matrix, Pex5p recycles to the cytosol through a process requiring monoubiquitination of a conserved, cytosolically exposed cysteine residue at the N-terminal region (Platta et al., 2016). The Pex5p recycling step requires ATP hydrolysis catalyzed by the AAA ATPases, Pex1p and Pex6p, and their membrane-anchoring peroxin, Pex26p (Matsumoto et al., 2003; Miyata and Fujiki, 2005; Platta et al., 2005; Tamura et al., 1998). Pex26p interacts with Pex14p to form a recycling complex with Pex5p, Pex6p, and Pex1p (Tamura et al., 2014). The Pex1p–Pex6p complex interacts with monoubiquitinated Pex5p to unfold the Pex5p polypeptide chain during the ATP-dependent extraction step from the translocation machinery (Pedrosa et al., 2018; Schwerter et al., 2018).

The membrane-anchored peroxin Pex14p has been described as a central component of the translocation machinery for peroxisomal matrix proteins (Dias et al., 2017). A conserved domain of Pex14p comprising residues 21–70 interacts with Pex5p, Pex13p, and Pex19p (Neufeld et al., 2009; Su et al., 2009). Pex14p forms a homodimer by the coiled-coil domain or a larger oligomer by GXXXG and AXXXA motifs in the transmembrane domain (Itoh and Fujiki, 2006).

Pex14p and Pex11p are a target for phosphorylation in yeast. In regard to Pex11p, cyclin-dependent protein kinase Pho85 is involved in the phosphorylation of Pex11p, negatively regulating the transfer of metabolites across peroxisomal membrane in

[1]Graduate School of Systems Life Sciences, Kyushu University, Fukuoka, Japan; [2]Faculty of Arts and Science, Kyushu University, Fukuoka, Japan; [3]Division of Organelle Homeostasis, Medical Institute of Bioregulation, Kyushu University, Fukuoka, Japan; [4]Institute of Rheological Functions of Food, Fukuoka, Japan; [5]Division of Cell Signaling, Fujii Memorial Institute of Medical Sciences, Tokushima University, Tokushima, Japan.

*K. Yamashita and S. Tamura contributed equally to this paper; Correspondence to Yukio Fujiki: yfujiki@kyudai.jp; Y. Yagita's present address is MRC Laboratory of Molecular Biology, Cambridge, UK.

yeast, *Saccharomyces cerevisiae* (Knoblach and Rachubinski, 2010; Mindthoff et al., 2016). Moreover, in *Hansenula polymorpha* (Tanaka et al., 2012), *Pichia pastoris* (Johnson et al., 2001), and *S. cerevisiae* (Oeljeklaus et al., 2016), Pex14p was detected in a phosphorylated and an unphosphorylated state. Additionally, although a lot of data on proteomics analysis show the phosphorylation sites of mammalian Pex14p, the role of Pex14p phosphorylation remains obscure.

On the other hand, the functions of protein import/trafficking in other organelles such as mitochondria or ER are regulated by the phosphorylation of these organelle assembly proteins in mitosis in many species, including yeast and mammalian cells (Harbauer et al., 2014; Olsen et al., 2010; Salazar-Roa and Malumbres, 2017; Shiota et al., 2015; Taguchi et al., 2007; Wang et al., 2014; Yeong, 2013). Protein trafficking from ER to Golgi apparatus is down-regulated by the phosphorylation of p47 with cyclin-dependent kinase 1 (CDK1) in mitosis in mammalian cells (Yeong, 2013). In *S. cerevisiae*, Tom6, a member of the translocase of the outer membrane (TOM) family, is phosphorylated in mitosis, resulting in up-regulation of the respiratory activity in mitochondria (Harbauer et al., 2014). Until now, the regulation of peroxisomal matrix protein import in mitosis has not been elucidated. Here we show that mammalian Pex14p is phosphorylated in mitosis, resulting in down-regulation of peroxisomal matrix protein import.

Results

Pex14p is phosphorylated in mitosis

It has been reported that Pex14p is phosphorylated in *P. pastoris*, *H. polymorpha,* and *S. cerevisiae* (Johnson et al., 2001; Oeljeklaus et al., 2016; Tanaka et al., 2012). According to at least two databases (PhosphoGRID, PhosphoSitePlus), yeast and mammalian Pex14p is also phosphorylated, whereas details of physiological functions of the phosphorylation are not yet known. Cell cycle–dependent regulation of mitochondrial components is observed in a few cases, including activation of the fission protein Drp1 and respiratory complex I (Harbauer et al., 2014; Taguchi et al., 2007; Wang et al., 2014).

In this study, we investigated whether Pex14p is phosphorylated in the mammalian cells HeLa and CHO-K1. One distinct slow-migrating band of Pex14p was detected in HeLa and CHO-K1 cells by Phos-tag PAGE, suggesting that Pex14p is partially phosphorylated in vivo (Fig. 1 A, lane 1). The results raised the possibility that Pex14p is phosphorylated in any specific cell events, including the cell cycle. HeLa and CHO-K1 cells were synchronized in mitosis with nocodazole, a microtubule-disrupting agent, and separated from adherent interphase cells by mitotic shake-off. In Phos-tag PAGE analysis, the slow-migrating Pex14p band was significantly increased in mitotic-phase cells compared with interphase cells (Fig. 1 A, lanes 2 and 3). An elevated level of phosphorylated histone (p-histone) indicated adequate separation of mitotic-phase cells. Upon treatment with λ protein phosphatase, the slow-migrating band was diminished in unsynchronized and mitotic cells (Fig. 1 A, lanes 4–6), suggesting that Pex14p is phosphorylated specifically in mitotic but not interphase cells. Various signal transduction pathways might be involved in the Pex14p phosphorylation. Next, we examined whether any other peroxins required for peroxisomal protein import are phosphorylated in mitosis. In mitotically arrested and interphase HeLa cells, no slow-migrating Pex13p was detected in Phos-tag PAGE analysis, while a part of Pex5p was likely to be phosphorylated, but independently of cell cycle progression. In mitotically arrested HeLa cells, most of the Pex14p was phosphorylated (Fig. 1 B), suggesting that the phosphorylation of Pex14p in the convergent import machinery is more likely involved in the regulation of peroxisomal protein translocation in mitotic cells.

Serine 232 of human Pex14p is phosphorylated in mitotic cells

To identify mitotic phosphorylation sites in human Pex14p, lysates from nocodazole-arrested and nontreated HeLa cells were subjected to immunoprecipitation with anti-Pex14p antibody followed by tryptic digestion and phosphopeptide enrichment by TiO_2. Liquid chromatography (LC)–tandem mass spectrometry (MS/MS) analysis showed that Pex14p phosphorylation at Ser232 was detected only in mitotic phase, suggesting that Ser232 is a phosphorylation site of endogenous human Pex14p in nocodazole-arrested, but not in nontreated, HeLa cells (Fig. 2, A and B). On the other hand, not only Ser232 but also Ser334 of Flag-tagged rat Pex14p transiently expressed in *pex14* HeLa cells were also identified as mitotic phosphorylation sites (Fig. 2, A and C). A mitotic phosphorylation site of human Pex14p, Ser232, was highly conserved between vertebrates, while the phosphorylation site of rat Pex14p, Ser334, was partially conserved (Fig. 2 D). These two serine residues are not conserved in yeast. These results suggest that Ser232 can be more important for mitotic phosphorylation and the functional regulation of Pex14p.

To confirm whether Ser232 and Ser334 of rat Pex14p are phosphorylated, these two sites were substituted for alanine, termed S232A and S334A, and the mitotic Pex14p was analyzed by Phos-tag PAGE analysis (Fig. 2 E). Pex14p-S232A was strongly suppressed in phosphorylation of Pex14p in mitotic HeLa cells, whereas Pex14p-S334A showed little effect on the mitotic phosphorylation of Pex14p. In addition, mutation of Ser232 to Ala appeared to induce mitotic phosphorylation of rat Pex14p at Ser247 (Fig. S1, lanes 4, 6, and 16). This residue of endogenous Pex14p was not phosphorylated in the mitotic HeLa cells, as assessed by LC-MS analysis. Ectopic transient expression of rat Pex14p harboring Ser232Ala appeared to cause an artifactual phosphorylation of Ser247 in mitotic cells. Ser232 residue of Pex14p comprises the Ser-Pro consensus sequence for phosphorylation by CDKs (Errico et al., 2010). Therefore, we verified which kinase is involved in the mitotic phosphorylation of Pex14p.

In mitosis, CDK1 phosphorylates various downstream proteins, thereby regulating mitosis-specific events. However, CDK1 should be inactivated to exit from mitosis, which could be achieved by protein phosphatases (Hunt, 2013). It is reasonable to suspect that mitosis-specific Pex14p phosphorylation is regulated by CDK1, because Pex14p is phosphorylated remarkably in mitosis rather than interphase. Thus, we investigated whether CDK1 is involved in Pex14p phosphorylation by making use of a CDK1 inhibitor, RO-3306. Mitotic HeLa cells were

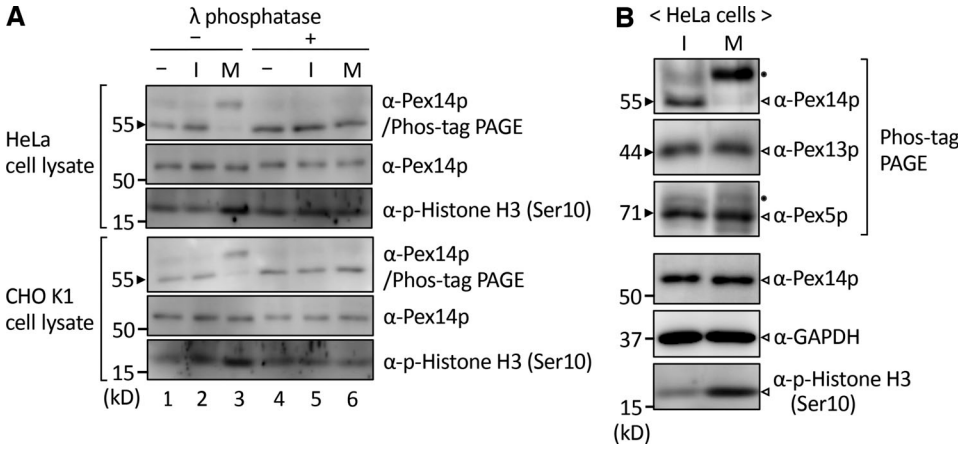

Figure 1. **Pex14p is phosphorylated in mitosis. (A)** HeLa and CHO-K1 cells at mitotic phase (M) and interphase (I) and nontreated cells (−) were lysed, treated with (+) or without (−) λ phosphatase, and analyzed by Phos-tag PAGE or SDS-PAGE followed by immunoblotting with anti-Pex14p antibody. Phosphorylated (p) histone H3, mitotic marker. **(B)** Lysates of HeLa cells at I and M were analyzed by Phos-tag PAGE (upper panels) or SDS-PAGE (lower panels) followed by immunoblotting with indicated antibodies. Open arrowheads indicate respective proteins; dots indicate a slow-migrating band.

incubated for 5–60 min with RO-3306 or control DMSO, and cell lysates were analyzed by Phos-tag PAGE. The slow-migrating phosphorylated Pex14p was no longer detectable, but not degraded, at least within 1-h treatment with RO-3306 (Fig. 2 F), suggesting that CDK1 is responsible for Pex14p phosphorylation. Because inhibition of CDK1 results in mitotic exit via activation of protein phosphatases (Wu et al., 2009), Pex14p is likely dephosphorylated by protein phosphatases that are activated at mitotic exit (Fig. 2 F, left panels). In addition, the phosphorylated Pex14p appeared to be stepwise dephosphorylated in the presence of RO-3306. Thus, it is likely that the inhibition of CDK1 with RO-3306 gives rise to dephosphorylation at Ser232 and subsequent phosphorylation at Ser247.

We next evaluated the knockdown effect of CDK1 on mitotic phosphorylation of Pex14p. Introduction of CDK1-specific siRNA knocked down >90% of CDK1 (Fig. 2 G). CDK1 down-regulation clearly decreased to a barely detectable level of the slow-migrating Pex14p band in Phos-tag PAGE analysis, in contrast to the mock-treated cells (Fig. 2 G, top panel). Taken together, these findings suggested that CDK1 is responsible for the mitotic phosphorylation of Pex14p.

Phosphomimetic mutation of Pex14p suppresses peroxisomal matrix protein import

Subcellular organelles receive mitosis-specific regulation. CDK1-mediated phosphorylation of mitochondrial proteins promotes their efficient protein import and thereby up-regulation of respiration, while the secretory pathway, including that from ER to Golgi apparatus, is down-regulated by CDK1 (Wang et al., 2014; Yeong, 2013). However, the regulation of peroxisomes in mitosis remains unknown. We next investigated mitosis-specific regulation on peroxisomal function by generating rat Pex14p mutants in which S232 and S334 were substituted by Asp to mimic phosphorylation, termed S232D and S334D. Peroxisome-restoring activity of S232D and a nonphosphorylation form, S232A, was verified by transient expression in the *pex14* HeLa cell line. In cells expressing WT *PEX14* or *S232A*, numerous PTS1-positive punctate structures, peroxisomes, were detected, indicating restoration of the impaired PTS1 protein import (Fig. 3 A, two-row upper panels). By contrast, Pex14p-S232D showed ∼70% activity in the PTS1 protein import assay (Fig. 3, A [upper panel] and Fig. 3 B). Moreover, catalase-positive peroxisomes were very weakly detected in the cells transfected with *S232D*, compared with those with *PEX14* and *S232A* (Fig. 3 A [two-row lower panels] and Fig. 3 B). The efficiency of catalase import was much lower than that of PTS1 import in the S232D-expressing cells. The difference in the import efficiency likely reflects the fact that Pex5p-catalase interaction is weaker than Pex5p binding to PTS1 (Maynard et al., 2004). With respect to Pex14pS334D, peroxisomal protein import was not suppressed (Fig. 3, A and B). Moreover, the import efficiency of a dual mutant Pex14pS232D/S334D was similar to that of S232D (Fig. S2), suggesting that S232 is an important phosphorylation site in the regulation of peroxisomal protein import during mitosis. Taken together, these data show that phosphomimetic mutation of Pex14p, S232D, suppresses peroxisomal protein import, i.e., down-regulation in mitosis.

To confirm this finding, we performed EGFP-PTS1 targeting assay using semi-intact HeLa cells that had been permeabilized with digitonin (Mukai et al., 2019). Cell staining at different stages of the cell cycle, prometaphase and interphase, represented a known pattern of mitotic spindle and DNA (Fig. 3 C, right panels). The shorter isoform of PTS1-receptor Pex5p, designated Pex5pS (Otera et al., 2002), was used in semi-intact cell import assays. After incubation of the semi-intact cells with the cytosol fraction containing recombinant EGFP-PTS1 and Pex5pS, EGFP-PTS1 was detected in a manner superimposable on Pex14p in interface cells (Fig. 3 C, right top panels, asterisks). By contrast, EGFP-PTS1 was not transported to peroxisomes in mitotic cells (Fig. 3 C, right top and middle panels, arrowheads). However, peroxisomal targeting of EGFP-PTS1 was restored in mitotic cells by treatment with λ phosphatase before the incubation of EGFP-PTS1 and Pex5pS-containing solution (Fig. 3 C, right middle and bottom panels). Similar observations were obtained with most other cells (not depicted). Therefore, it is

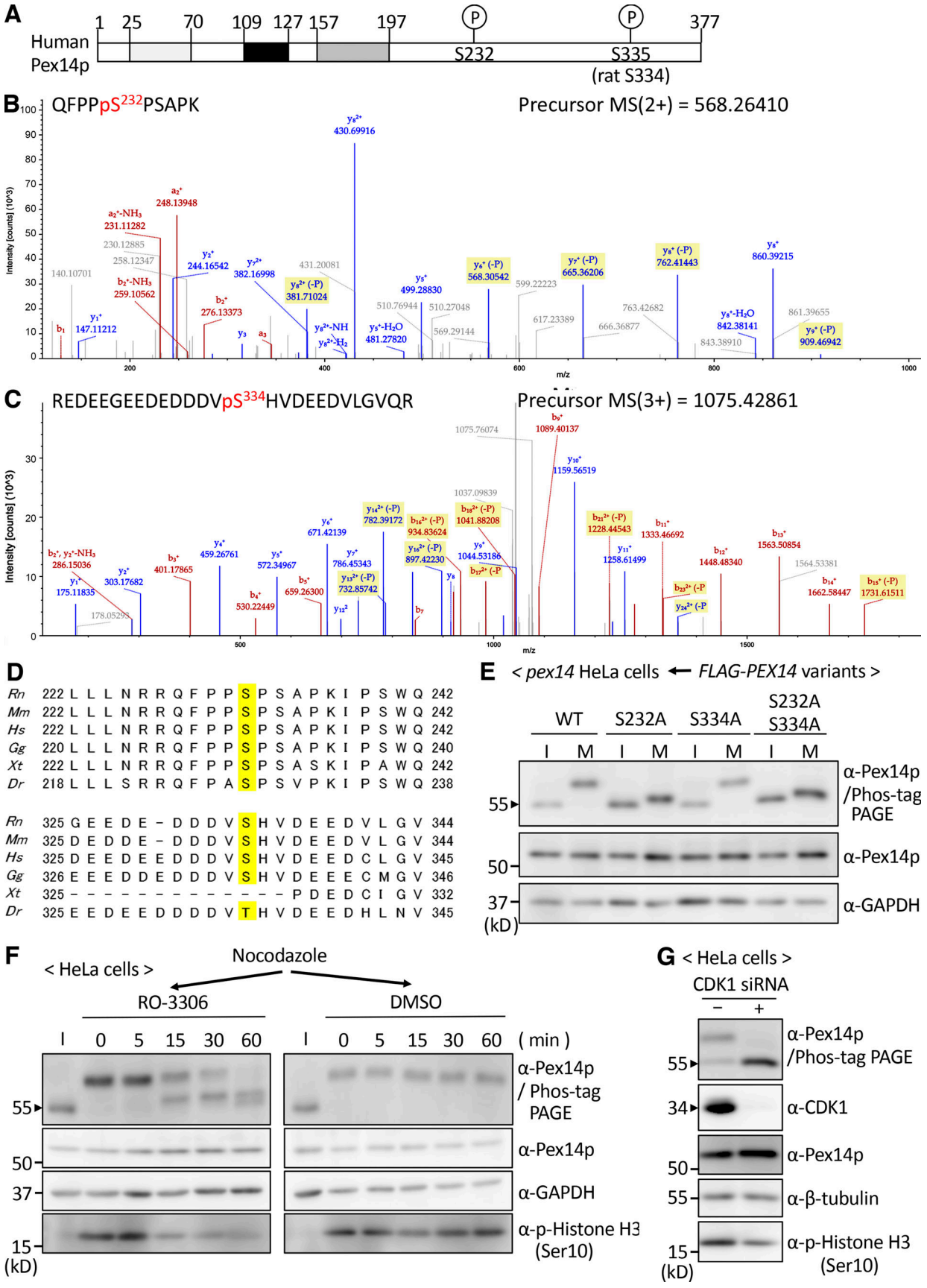

Figure 2. **Mitotic phosphorylation of Pex14p. (A)** Schematic representation of full-length human Pex14p with mitotic phosphorylation sites, S232 and S335. Light gray box, Pex5p-binding domain; black box, transmembrane domain; dark gray box, coiled-coil domain. **(B)** MS analysis of phosphorylated Pex14p in

mitotic HeLa cells. HeLa cells were treated for 12–18 h with 50 ng/ml nocodazole and collected by mitotic shake-off. Adherent cells after shake-off were collected as interphase cells. Endogenous Pex14p in mitotic and interphase HeLa cells was immunoprecipitated with anti-Pex14p antibody followed by tryptic digestion and phosphopeptide enrichment by TiO_2. Phosphorylation of Ser232 was demonstrated by the MS/MS spectrum of the 568.2641 ion from mitotic cells. **(C)** FLAG-tagged rat Ptex14p in mitotic and interphase *pex14* HeLa cells was immunoprecipitated with anti-FLAG antibody followed by tryptic digestion. Phosphorylation of Ser334 was demonstrated by the MS/MS spectrum of the 1075.42861 ion from mitotic cells. **(D)** Multiple alignments of the region encompassing mitotic phosphorylation sites in Pex14p are shown. Yellow box indicates conserved Ser/Thr. *Rn*, *Rattus norvegicus* (rat); *Mm*, *Mus musculus* (mouse); *Hs*, *Homo sapiens* (human); *Gg*, *Gallus gallus* (chicken); *Xt*, *Xenopus tropicalis* (frog); *Dr*, *Danio rerio* (zebrafish). **(E)** WT Pex14p and its mutants each harboring S232A, S334A, and S232A plus S334A were separately expressed in *pex14* HeLa cells. Mitotic-phase and interphase cells were separated and analyzed by Phos-tag PAGE or SDS-PAGE, followed by immunoblotting with anti-Pex14p antibody. GAPDH, loading control. **(F)** Mitotic HeLa cells arrested with nocodazole were treated for 5–60 min with CDK1 inhibitor RO-3306 or DMSO. Respective cell lysates were analyzed by Phos-tag PAGE (top panels) or SDS-PAGE followed by immunoblotting with indicated antibodies. I, cell lysate from interphase cells. **(G)** HeLa cells were treated for 72 h with control siRNA (–) or CDK1 siRNA (+). Lysates of nocodazole-treated HeLa cells were analyzed by Phos-tag PAGE (top panel) or SDS-PAGE followed by immunoblotting with antibodies indicated on the right. β-Tubulin, loading control.

likely that the mitotic phosphorylation of Pex14p is responsible for the suppression of peroxisomal protein import.

Pex5p binding to Pex14p is not altered in mitosis

As described above, we showed that phosphorylation of Pex14p suppressed catalase and PTS1 import in mitotic cells (Fig. 3, A and B). Pex14p acts as an initial docking factor of Pex5p, the cytosolic receptor of PTS1 proteins. Next, we examined whether such phosphorylation influences the interaction of Pex14p with Pex5p. FLAG-Pex14p, S232A, or S232D was expressed in *pex14* HeLa cells. Cell lysates of these transformants were analyzed by immunoprecipitation assay with anti-FLAG antibody. Approximately the same level of endogenous Pex5p was coimmunoprecipitated with FLAG-Pex14p, S232A, and S232D (Fig. 4 A). Furthermore, we performed immunoprecipitation studies using the lysates of HeLa cells at mitosis and interphase. Pex5p was almost equally coimmunoprecipitated with Pex14p from the mitotic-phase and interphase cells with the antibody specific for the N-terminal part of Pex14p, Pex14pN, indicating that both phosphorylated and unphosphorylated Pex14p are equally competent to interact with Pex5p (Fig. 4 B).

Pex5p is imported into peroxisomes in interphase and mitotic cells

To assess whether Pex5p import into peroxisomes is altered in mitotic cells, we performed in vitro Pex5p import assays using ^{35}S-labeled Pex5pL, a longer isoform of Pex5p. With postnuclear supernatant (PNS) fractions each from interphase and mitotic HeLa cells, [^{35}S]Pex5pL was detected in both organelle fractions, suggesting that [^{35}S]Pex5pL was imported into peroxisomes (Miyata and Fujiki, 2005) in mitosis as in interphase as assessed by proteinase K resistance (Fig. 5 A, top panel, lanes 2 and 5, solid arrowhead). A partially cleaved form of protease-resistant [^{35}S]Pex5pL was also detected in the organelle fraction from interphase cells (Fig. 5 A, top panel, lane 2, open arrowhead), likely representing [^{35}S]Pex5pL locating in the peroxisomal membrane and partly accessible to the protease (Miyata and Fujiki, 2005). This result suggests that a part of Pex5p in peroxisomes is exposed to cytosol. The N-terminal region of Pex5p, which is accessible to monoubiquitination leading to Pex5p release to the cytosol by Pex1p and Pex6p, is exposed to the cytosol, consistent with the finding that the N-terminal region of Pex5p is partially digested with proteinase K (Dias et al., 2017; Gouveia et al., 2003; Pedrosa et al., 2018). In the organelle fraction from mitotic cells, however, the partially cleaved [^{35}S]Pex5pL was not detectable, suggesting that a part of [^{35}S]Pex5pL was not exposed to the cytosol (Fig. 5 A, top panel, lane 5, solid arrowhead). Imported Pex5p was not cleaved with proteinase K in mitosis, suggesting that Pex5p is imported into and retained in peroxisomes in the mitotic phase of the cell cycle. These results raise the question of whether the step of Pex5p recycling is suppressed in mitosis.

Pex5p export is suppressed in mitotic cells

Next, we investigated whether Pex5p is exported from peroxisomes in mitotic cells. The export reaction mixtures containing [^{35}S]Pex5pL-imported organelle fraction (Fig. 5 A, lanes 1 and 4) were incubated at 26°C for 30 min and separated into organelle pellet (P) and cytosolic supernatant (S) fractions. [^{35}S]Pex5pL was detected in the S fraction with concomitant decrease of [^{35}S]Pex5pL in the P fraction from interphase cells, suggesting that Pex5p was exported from peroxisomes, whereas [^{35}S]Pex5pL export was barely detected in the case of mitotic cells (Fig. 5 B, top panel, lanes 2 and 4). [^{35}S]Pex5pL in S and P fractions was quantified to verify the Pex5p export (Fig. 5 C). The organelle and cytosolic fractions were separated and verified for phosphorylation of Pex14p and Pex14p levels by Phos-tag PAGE and SDS-PAGE, both followed by immunoblotting (Fig. 5 B, middle and bottom panels). These results suggested that Pex5p export to the cytosol is suppressed in mitosis, although Pex5p is normally imported into peroxisomes (Fig. 5 C). Taken together, these data show that the N-terminal region of Pex5p is not exposed to the cytosol in mitosis, and probably the Pex5p structure is not altered for Cys monoubiquitination, thereby resulting in inhibition of the interaction between Pex1p/Pex6p and Ub-Pex5p through ubiquitin moiety (Pedrosa et al., 2018; Schwerter et al., 2018). In mitosis, Pex5p export from peroxisomes is likely suppressed by the mitotic phosphorylation of Pex14p.

Pex14p phosphorylation enhances its dimerization via the coiled-coil domain

The coiled-coil domain is mainly responsible for homodimerization of Pex14p (Fransen et al., 2002; Itoh and Fujiki, 2006). In this study, we investigated whether mitotic phosphorylation influences the homomeric interaction of Pex14p and alters peroxisomal import of matrix proteins. The efficiency of homomeric interaction was evaluated with FLAG- or His-tagged full-length Pex14p and respective variants harboring S232A

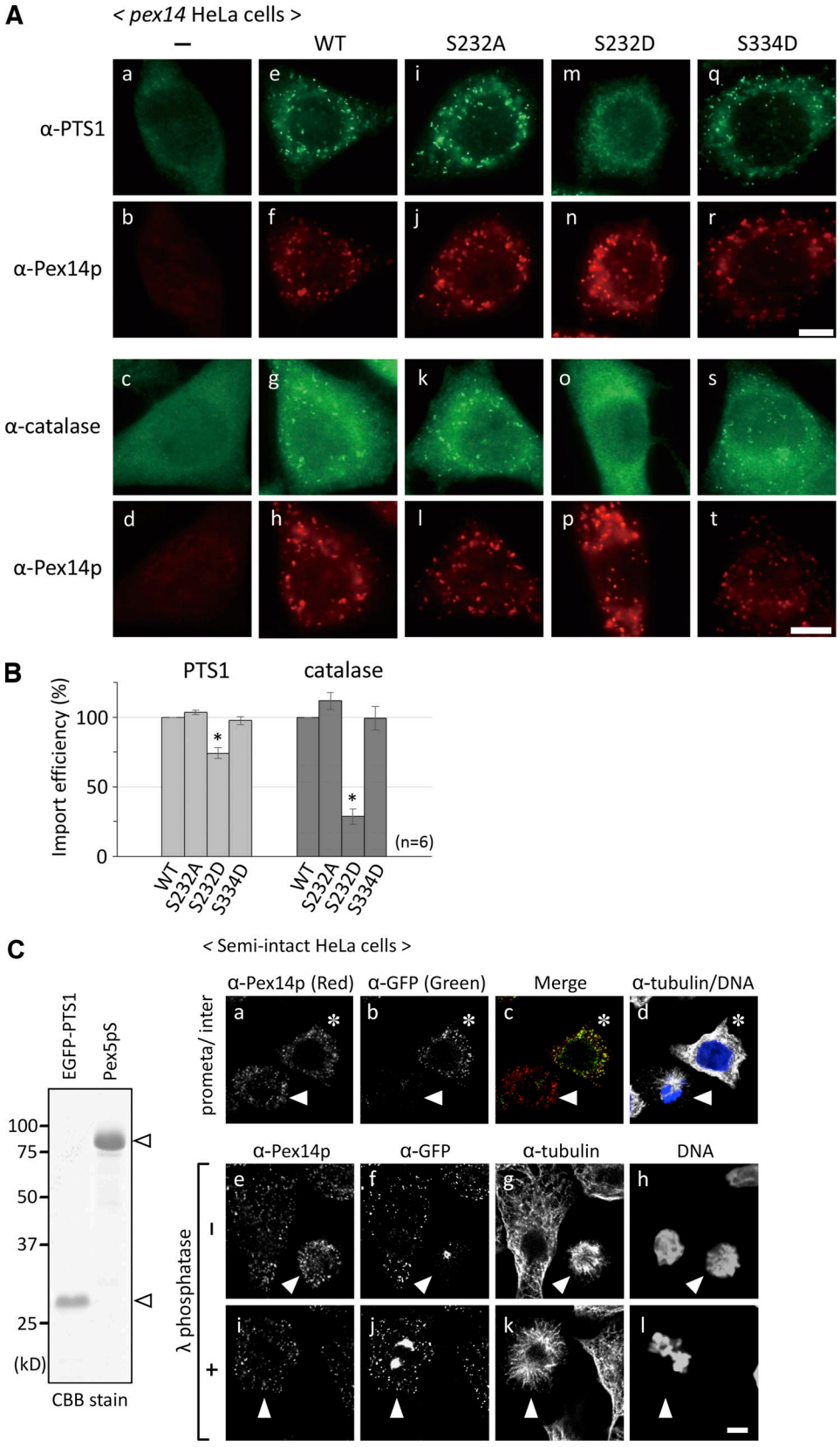

Figure 3. **Peroxisomal protein import in mitotic HeLa cells. (A)** Morphological analysis of phosphomimetic mutants of Pex14p. *pex14* HeLa cells each expressing mock (a–d), FLAG-Pex14p WT (e–h), S232A (i–l), S232D (m–p), and S334D (q–t) were fixed and visualized by staining with indicated antibodies 24 h after transfection. Scale bar, 5 µm. **(B)** Import efficiency is represented as percentages of PTS1- or catalase-discernible cells in Pex14p-positive cells. $n = 6$. Statistical significance was verified by ANOVA and post hoc Dunnett's test, and the significance is presented by asterisk (*, $P < 0.001$). Error bars show SEM.

(C) EGFP-PTS1 import assay was performed with semipermeabilized HeLa cells. Left: Purified recombinant proteins, EGFP-PTS1 (0.5 µg) and Pex5pS (2 µg), were verified by SDS-PAGE and Coomassie Blue staining. Open arrowheads indicate respective proteins. Right top: EGFP-PTS1 and Pex5pS (1 ng each) were incubated at 4°C for 1 h in the semi-intact import buffer and assessed for peroxisomal import at 26°C for 1 h using semi-intact HeLa cells as described (Mukai et al., 2019). Cells were stained with antibodies to Pex14p (a, e, and i), GFP (b, f, and j), and β-tubulin (g and k), and DNA was stained with Hoechst 33342 (h and l). Merged view of images stained with anti-Pex14p and anti-GFP antibodies and tubulin-stained plus Hoechst 33342–stained nuclei are shown in c and d, respectively. Right middle and bottom: Semi-intact HeLa cells were treated with (+) or without (–) λ protein phosphatase (λ phosphatase) in phosphatase treatment buffer containing 1 mM $MnCl_2$. EGFP-PTS1 import assay was likewise performed as in the top panels. Solid arrowheads indicate prometaphase cells; asterisks show interphase cells. Scale bar, 5 µm.

(SA) or S232D (SD) mutations (Fig. 6 A). FLAG- and His-tagged Pex14p or the mutants were coexpressed in *pex14* HeLa cells and verified for homointeraction by coimmunoprecipitation assay with anti-FLAG antibody. Nearly an equal amount of WT and S232A- and S232D-mutated His-Pex14p was recovered in the fractions bound to respective FLAG-Pex14p variants, suggesting that SA and SD mutations did not alter the efficiency of homomeric interaction (Fig. 6 B). Next, N-terminally truncated FLAG- or HA-tagged Pex14p(156–376) with or without S232 mutations were likewise assessed for homomeric interaction as in Fig. 6 B. HA-Pex14p(156–376) variants recovered in the fractions bound to FLAG-Pex14p(156–376) were analyzed. Interestingly, HA-Pex14p(156–376)SA was coimmunoprecipitated with FLAG-Pex14p(156–376)SA at a level similar to that noted with WT Pex14p(156–376), whereas the recovery of HA-Pex14p(156–376)SD by immunoprecipitation with FLAG-Pex14p(156–376)SD was higher, suggesting that phosphomimetic mutation enhances homointeraction between HA- and FLAG-tagged Pex14p(156–376) (Fig. 6 C). Taken together, these data show that the effect of phosphorylation is likely restricted to the region proximal to S232 of Pex14p.

Next, we assessed the effect of phosphomimetic mutation on homo-oligomerization of Pex14p(156–376) by blue native PAGE (BN-PAGE) analysis. FLAG-Pex14p(156–376) was detected as a homo-oligomer, consistent with the results in the coimmunoprecipitation studies and our earlier report (Fig. 6 D; Itoh and Fujiki, 2006; Fransen et al., 2002). Moreover, homo-oligomerization was stabilized by phosphomimetic mutation of FLAG-Pex14p(156–376)SD. Quantified data showed that the formation of SD mutant homo-oligomer was increased ∼1.5-fold compared with that of WT or SA mutant (Fig. 6 D, right panel). Moreover, another N-terminally truncated Pex14p variant, FLAG-Pex14p(200–376), was also competent to form homo-oligomer despite lacking the coiled-coil domain (Fig. 6 E). It is noteworthy that the homo-oligomer of SD mutant migrated slightly faster than that of WT or SA mutant, where these homo-oligomers were detected at a similar level (Fig. 6 E). Phosphorylation at S232 likely modulates Pex14p homointeraction by converting the homo-oligomer to a more compact conformation. This conformational change of homo-oligomer was more readily observed upon deletion of a coiled-coil domain. Taken together, these data show that it is more likely that the phosphorylation at S232 enhances the homomeric interaction and stabilizes the homo-oligomer of Pex14p C-terminal part.

These results raised the question of whether Pex14p changes domain structure or membrane topology in response to the phosphorylation at S232. Therefore, we used the limited proteolysis method to assess any conformational changes of Pex14p induced by phosphorylation at S232. PNS fractions from *pex14* HeLa cells expressing WT, SA, and SD mutants of FLAG-Pex14p(156–376) were treated with various concentrations of proteinase K. Upon proteinase K treatment, WT and SA mutants of FLAG-Pex14p(156–376) resulted in several smaller-mass

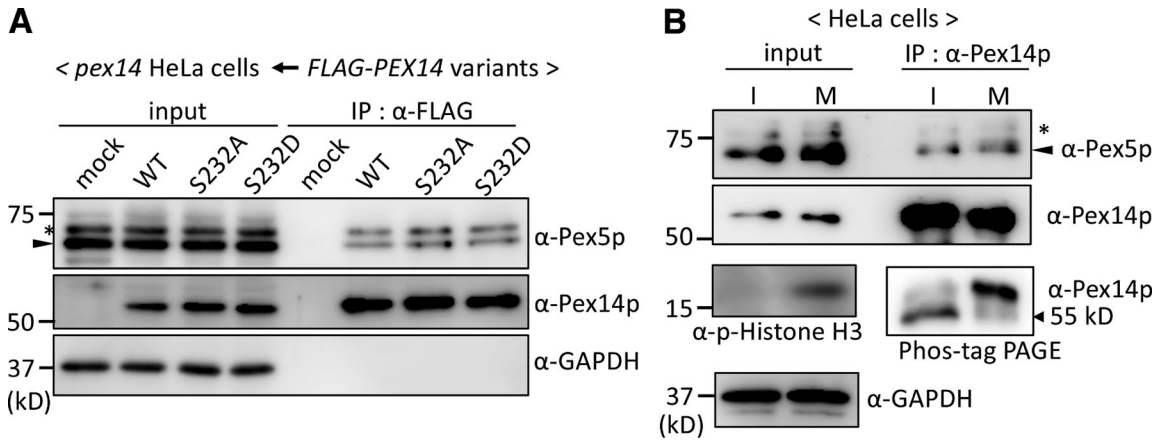

Figure 4. **Pex5p binding to Pex14p is not altered in mitosis. (A)** Coimmunoprecipitation assay using FLAG-Pex14p variants with Pex5p. WT FLAG-Pex14p and its mutants each harboring S232A and S232D were separately expressed in *pex14* HeLa cells, and cell lysates were subjected to immunoprecipitation (IP) with anti-FLAG antibody. Input, 10% input used for IP. Immunoprecipitated proteins were analyzed by SDS-PAGE and immunoblotting using antibodies to Pex5p (top), Pex14p (middle), and GAPDH (bottom). Arrowhead indicates Pex5p; asterisk indicates a nonspecific band. **(B)** The binding of endogenous Pex14p to Pex5p in mitosis. Lysates from mitotic (M) and interphase (I) HeLa cells were subjected to IP with anti-Pex14p antibody. Input, 5% input used for immunoprecipitation. Immunoprecipitates were analyzed by SDS-PAGE and Phos-tag PAGE followed by immunoblotting with antibodies to Pex5p, Pex14p, p-histone H3, and GAPDH. Arrowhead indicates Pex5p in SDS-PAGE and Pex14p in Phos-tag PAGE; asterisk indicates a nonspecific band.

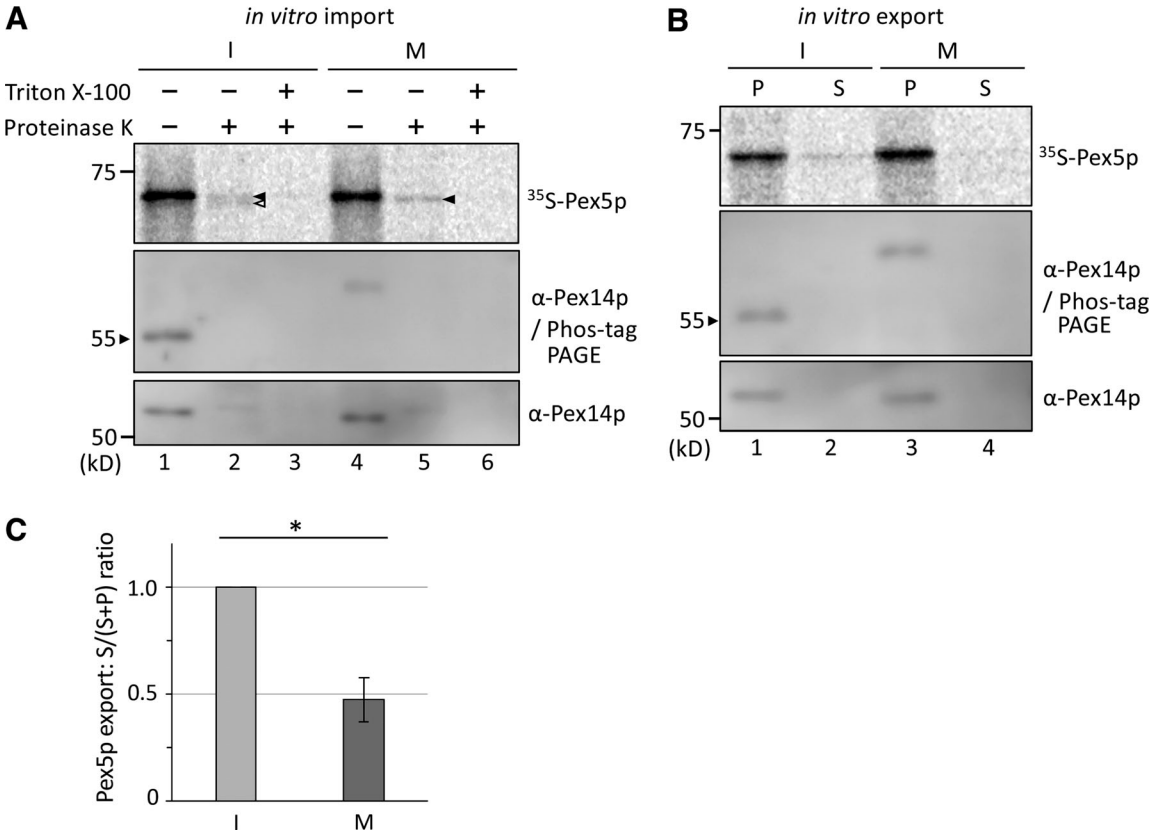

Figure 5. **In vitro Pex5p import and export assays. (A)** An in vitro Pex5p import assay was performed. [^{35}S]Pex5pL was incubated with PNS fractions each from HeLa cells at mitotic phase (M) or interphase (I). After incubation, the reaction mixtures were mock treated (lanes 1 and 4) or treated with 40 µg/ml proteinase K for 30 min at 0°C (lanes 2, 3, 5, and 6) in the absence (–) or presence (+) of 1% Triton X-100 and were then separated to organelle (P) and cytosolic (S) fractions by centrifugation. Proteinase K digestion was terminated, and aliquots of P fractions were analyzed by SDS-PAGE (top and bottom) and Phos-tag PAGE (middle). [^{35}S]Pex5pL was detected by an FLA7000 autoimaging analyzer. Pex14p was detected by immunoblotting. Solid and open arrowheads indicate full-length and partially proteinase K-cleaved [^{35}S]Pex5pL, respectively. In Phos-tag PAGE, solid arrowhead indicates intact Pex14p. **(B)** In vitro export of Pex5p. ^{35}S-Pex5L import was performed with PNS from HeLa cells at M or I, as in A. The P fractions (A, lanes 1 and 4) were centrifuged and resuspended with the S fraction in export buffer containing 3 mM ATP. The reaction mixtures were incubated at 26°C for 30 min and centrifuged to separate into P and S fractions. [^{35}S]Pex5pL in P and S fractions was separated by SDS-PAGE and detected by a Typhoon FLA 9500 autoimaging analyzer (top). Endogenous Pex14p was separated by Phos-tag PAGE (middle) or SDS-PAGE (bottom) and detected by immunoblotting. In Phos-tag PAGE, solid arrowhead indicates intact Pex14p. **(C)** Results obtained in B were represented as ratios of [^{35}S]Pex5pL export activities. [^{35}S]Pex5pL in S and P fractions was quantified and shown as ratios of S/total (S plus P), n = 3. Statistical significances were verified by Student's t test, and the significance is presented with asterisk (*, $P < 0.05$).

fragments compared with the SD mutant, suggesting that the N-terminal region of the SD mutant was more resistant to the proteinase K digestion. We interpreted the results to mean that this region containing the coiled-coil domain shifts to a more compact and protease-resistant configuration upon phosphorylation at S232 (Fig. 6 F). Accordingly, it is conceivable that phosphorylation at S232 induces a conformational change and stabilization of Pex14p homo-oligomer via the coiled-coil domain (Fig. 6 G).

Mitotic phosphorylation protects the N-terminal region of Pex14p from protease digestion

We likewise performed limited proteolysis analysis as in Fig. 6 F to verify the conformational change of Pex14p in mitotic cells. PNS fractions each from interphase and mitotic HeLa cells were treated with proteinase K and analyzed by immunoblotting with antibody to Pex14p N-terminal region. N-terminal region of Pex14p from interphase cells resulted in several lower-molecular-mass fragments, whereas that from metaphase cells was more resistant to the partial digestion, implying that the N-terminal region of Pex14p was converted to a more protease-resistant conformation (Fig. 7 A, left panel). Moreover, Pex14p fragments with lower molecular masses were not detected with antiserum specific for the C-terminal region (Fig. 7 A, right panel, and Fig. S3). Taken together, these results suggest that mitotic phosphorylation of Pex14p leads to a conformational change of its C-terminal part containing the coiled-coil domain. Moreover, it is likely that structural changes in the C-terminal part of Pex14p translate to changes in the N-terminal region of Pex14p, which is the part of the Pex5p-binding domain, leading to reduced Pex5 export from the peroxisomal matrix to the cytosol, and thereby overall suppression of peroxisomal matrix protein import.

Discussion

Peroxisomal matrix proteins are posttranslationally imported into peroxisomes by a membrane-bound translocation complex

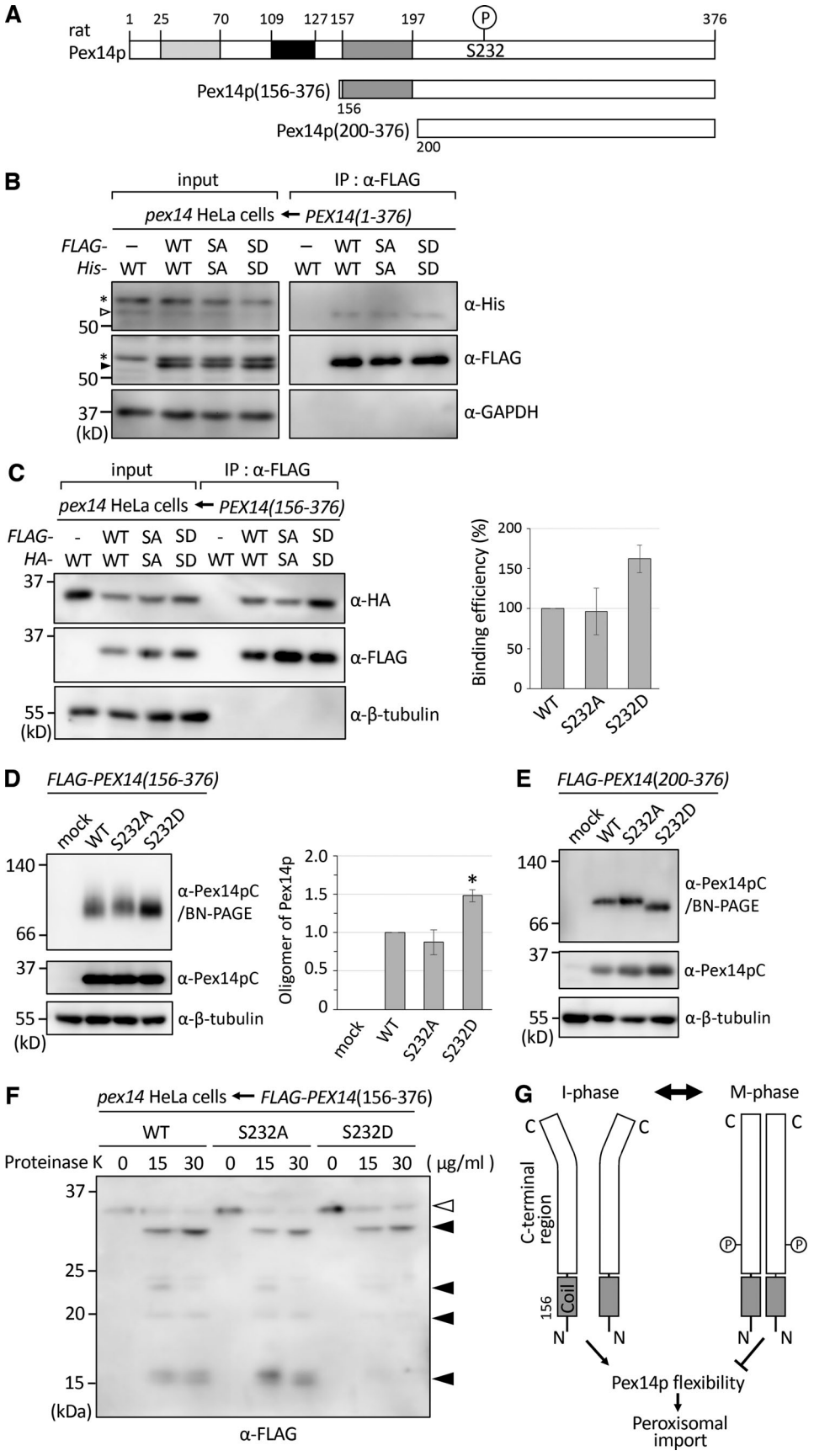

Figure 6. **Dimerization of Pex14p C-terminal domain. (A)** Schematic representation of rat Pex14p variants. Numbers, amino acid residue positions of Pex14p; light gray box, Pex5p binding domain; solid box, transmembrane domain; dark gray box, putative coiled-coil domain. S232 was substituted by A or D in

the truncated mutant of Pex14p, Pex14p(156–376), and Pex14p(200–376). **(B)** FLAG-tagged full-length Pex14p(1–376) and its variants harboring S232A (SA) or S232D (SD) mutation were coexpressed with His-tagged Pex14p(1–376) variants in *pex14* HeLa cells. Immunoprecipitates using anti-FLAG antibody were analyzed by SDS-PAGE and immunoblotting with antibodies to His (top) and FLAG (middle). GAPDH, loading control. Input, 10% input used for immunoprecipitation (IP). Open and solid arrowheads indicate the His-Pex14p and FLAG-Pex14p, respectively; asterisk indicates a nonspecific band. **(C)** Left: FLAG- and HA-tagged Pex14p(156–376) with or without S232 mutations were assessed for homointeraction in *pex14* HeLa cells as in B. Immunoblotting with antibodies to HA (top) and FLAG (middle). β-Tubulin, loading control. Input, 5% input used for IP. Right: The binding efficiency is represented as percentages of HA-tagged Pex14p(156–376) to FLAG-tagged Pex14p(156–376). Values are the averages from two experiments. Error bars show range. **(D)** Left: WT Pex14p and mutant Pex14p(156–376) were expressed in *pex14* HeLa cells. Lysates from these cells were analyzed by BN-PAGE and SDS-PAGE. An oligomer was detected by immunoblotting with anti-Pex14pC antibody (top). Immunoblot analyses with anti-Pex14pC (middle) and anti-β-tubulin (bottom) antibodies were examined to assess loading controls. Molecular mass markers are on the left. Right: Oligomer of Pex14p(156–376) was quantified and normalized with the loaded amount in BN-PAGE analysis. Homo-oligomerization was represented by taking as 1 that of Pex14p(156–376), and evaluated as bar graph (n = 2). Error bars showed standard error of the averages. Statistical significance in n = 2 between WT and S232D was verified by ANOVA and post hoc Dunnett's test, and the significance is presented by asterisk (*, $P < 0.05$). **(E)** WT Pex14p and mutant Pex14p (200–376) were expressed in *pex14* HeLa cells. Lysates from these cells were separated by BN-PAGE and SDS-PAGE followed by immunoblotting as described in D. An oligomer of Pex14p (200–376) was detected (top) as in D. **(F)** FLAG-Pex14p (156–376) or its variants harboring S232A or S232D mutation was expressed in *pex14* HeLa cells. PNS fractions from these cells were treated for 30 min on ice with proteinase K at the indicated concentration. The reaction mixtures were analyzed by SDS-PAGE and immunoblotting with anti-FLAG antibody. Open and solid arrowheads indicate the FLAG-Pex14p (156–376) and major proteinase K–digested fragments, respectively. **(G)** A schematic model of conformational change in Pex14p C-terminal region (represented as a homodimer), between interphase (I-phase) and mitotic phase (M-phase). The C-terminal region following the transmembrane domain was presented. Shaded box, coiled-coil domain (156–197); bar, C-terminal region encompassing 200–376. Phosphorylation at S232 suppresses the flexibility of C-terminal region and confers a conformational change of Pex14p.

comprising membrane peroxin Pex14p as a major component (Barros-Barbosa et al., 2019; Itoh and Fujiki, 2006; Oliveira et al., 2002; Otera et al., 2002; Reguenga et al., 2001). We earlier reported that Pex14p forms a homodimer via the coiled-coil domain and interacts with Pex5p, Pex13p, and Pex19p (Itoh and Fujiki, 2006; Tamura et al., 2014). Pex14p homo-oligomer is likely to be involved in the assembly of pore-like structures at the peroxisomal membrane (Meinecke et al., 2016). Here we investigated peroxisomal protein import and its dynamics in mitotic HeLa cells. In mitosis, Pex14p is specifically phosphorylated at Ser-232, resulting in down-regulation of peroxisomal protein import. The mitotic phosphorylation site of human Pex14p, S232, fits to a consensus motif, P-X-S-P, for CDK1 and is highly conserved among vertebrates (Fig. 2 D), but not in fly, worm, or yeast. This is the first demonstration for the regulation of peroxisome matrix protein translocation via signal transduction pathways responding to intra- or extracellular signals. In the present study, we show that N-terminal deletion variants, FLAG-Pex14p(156–376) and FLAG-Pex14p(200–376), are sufficient for homointeraction to assemble a homo-oligomer.

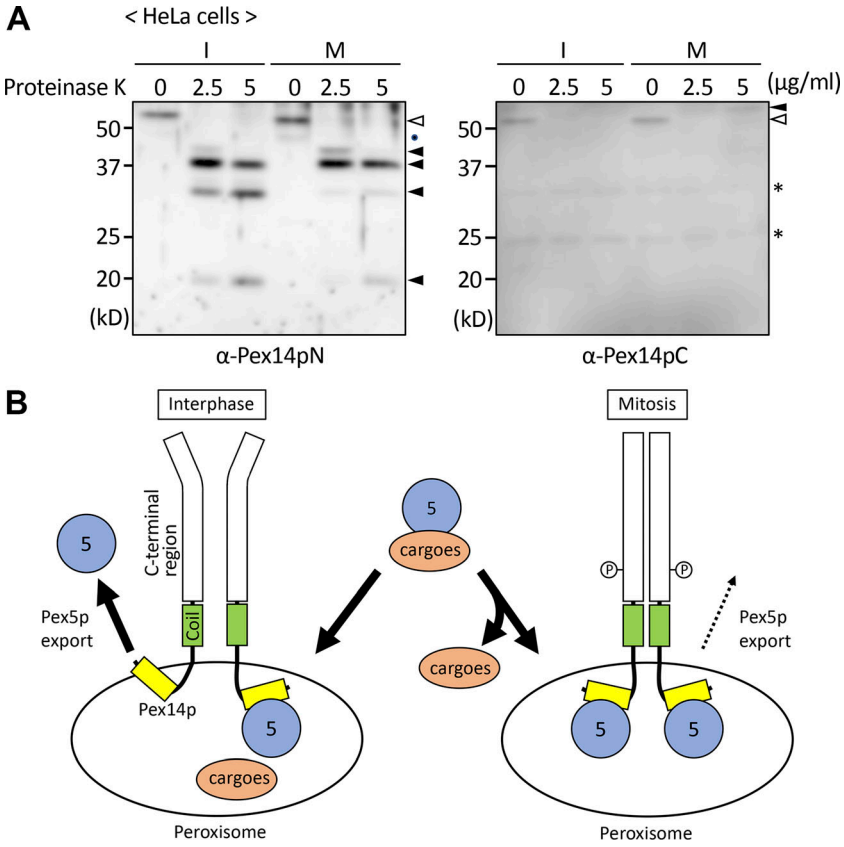

Figure 7. **Conformational changes of Pex14p in cell cycle progression. (A)** PNS fractions from interphase (I) and mitotic phase (M) HeLa cells were treated for 30 min on ice with proteinase K at indicated concentrations. The reaction mixtures were analyzed by SDS-PAGE and immunoblotting with antibodies to Pex14pN (left) and Pex14pC (right). Open and solid arrowheads indicate the endogenous Pex14p and major proteinase K–digested fragments, respectively. The dot designates a cleaved product of Pex14p; *, nonspecific bands. Right, solid arrowhead indicates an unknown band. **(B)** A model for the Pex14p conformations regulated by phosphorylation at S232. Pex5p-cargo complexes in interphase and mitotic-phase cells are competent for targeting to peroxisomes. Phosphorylated Pex14p at S232 in mitotic cells shows relatively compact and less flexibility. This conformational change potentially suppresses the mobility of Pex5p-binding domain at N-terminal region of Pex14p, thereby giving rise to the retardation of Pex5p recycling in mitotic cells.

It is more likely that the C-terminal part of Pex14p possesses several homomerically interacting domains as well as the coiled-coil domain and undergoes conformational change by mitotic phosphorylation, resulting in an increase of homomeric-interacting affinity. Recently, Pex14p was suggested to expose its N-terminal domain into the organelle matrix (Barros-Barbosa et al., 2019). Accordingly, it is possible that the protease-sensitive form exposing its Pex5p binding domain to cytosol is responsible for the step of Pex5p recycling in interphase cells. In this study, we verified the involvement of mitotic Pex14p phosphorylation in the export step of Pex5p. Intriguingly, we revealed that peroxisomes from interphase cells are competent to export Pex5p into the cytosol, whereas mitotic peroxisomes barely export Pex5p. These findings suggest that mitotic phosphorylation of Pex14p suppresses the topological change of the N-terminal part, resulting in the down-regulation of Pex5p export. The question to be addressed is how the phosphorylation of the Pex14p C-terminal part leads to a stabilization of homo-oligomer and suppression of the Pex5p export step. The mechanistic roles of phosphorylation in the peroxin–peroxin interaction and Pex5p export reaction remain to be defined.

Synchronization of cytoplasmic and nuclear events is temporally and spatially regulated by CDK1 during G2/M progression (Barnes et al., 2001). The nuclear envelope and Golgi apparatus are disassembled in early mitotic phase and then reconstructed at a late stage of mitosis (Smoyer and Jaspersen, 2014). Soluble factors including p97 and p47 involved in Golgi assembly are phosphorylated during mitosis and promote mitotic Golgi disassembly. Furthermore, dynamin-related GTPase, Drp1, is phosphorylated by CDK1, which stimulates mitochondrial fission in mitosis (Taguchi et al., 2007). Several assembly factors of Golgi apparatus and mitochondria such as p47 and Tom6, respectively, are phosphorylated and regulated in mitosis for cell cycle progression (Uchiyama et al., 2003; Harbauer et al., 2014). It is reasonable to speculate that mitosis-specific functions such as chromosome separation and cytokinesis are selected and prioritized, whereas peroxisomal protein transport and metabolic functions are suppressed by the phosphorylation of Pex14p. An elevated level of Pex5p associated with Pex14p is detectable under ATP-limiting conditions, and ATP depletion fails to export Pex5p from peroxisomes (Miyata and Fujiki, 2005; Platta et al., 2005). In the present study, Pex5p export was indeed significantly lowered in mitotic peroxisomes, suggesting that peroxisomal protein import is down-regulated and suppressed in order not to consume ATP (Fig. 5 B).

We recently reported that a portion of catalase is localized to the cytosol at steady state in WT CHO-K1 cells, suggesting that cytosolic catalase could more efficiently eliminate oxidative stress than peroxisomal catalase (Hosoi et al., 2017). The mitotic phosphorylation of Pex14p suppresses peroxisomal import, resulting in a lower efficiency of catalase import to peroxisomes compared with that of the other matrix proteins, including PTS1 proteins (Fig. 3, A and B). In mitotic cells, the inefficient import of catalase to peroxisomes would increase cytosolic catalase, which eliminates the cytosolic reactive oxygen species including H_2O_2. DNA is thought to be fragile and sensitive to oxidative stress, such as hydrogen peroxide, especially in mitosis, in which the nuclear envelope disappears. A reduced level of cytosolic catalase in mitosis might increase the risk of DNA damage from hydrogen peroxide. Dubreuil et al. (2020) recently reported that cytosolically localized catalase is the most protective in cells against the treatment with H_2O_2, implying that the localization of catalase in the cells determines its efficiency in ameliorating oxidative stress. Moreover, cell cycle–dependent phosphorylation of Pex14p may also be involved in the regulation of peroxisomal assembly and metabolic function in embryonic development with rapid and intense cell division.

Here we propose a model for the role of mitotic phosphorylation of Pex14p in peroxisomal matrix protein import. The Pex5p–cargo protein complex targets to peroxisomes through its binding to the docking complex containing Pex14p. Pex5p is competent to interact with unphosphorylated and phosphorylated Pex14p. In nonmitotic cells, cargo proteins are unloaded from Pex5p inside or at the surface of peroxisomes, and conformational change of Pex14p more likely leads to Pex5p release from Pex14p and its export from peroxisomes. On the other hand, in mitotic cells, S232 phosphorylation of Pex14p prevents topological change of the N-terminal part of Pex14p, resulting in the suppression of Pex5p export and peroxisomal matrix protein import.

Materials and methods

Antibodies

We used guinea pig antisera to C-terminal region of rat Pex14p, termed Pex14pC (Mukai et al., 2002), and rabbit antisera to N-terminal part of rat Pex14p, named Pex14pN (Shimizu et al., 1999), as well as Pex14pC (Shimizu et al., 1999), PTS1 peptide (Otera et al., 2002), human catalase (Matsumoto et al., 2003), Pex13pSH3 (Mukai and Fujiki, 2006), and Pex5p (Okumoto et al., 2011). Rabbit antibodies to FLAG (F7425) and β-tubulin were purchased from Sigma-Aldrich; rabbit anti-GFP was from MBL; rabbit monoclonal antibody to CDK1 was from Abcam; mouse antibody to phospho-histone H3 (Ser10; D2C8) was from Cell Signaling Technology; mouse antibody to GAPDH (3E12) was from Bioss; mouse antibody to HA (16B12) was from Covance; and mouse antibody to His_6 (34660) was from Qiagen. For immunoprecipitation, we used mouse anti-Flag M2 agarose (Sigma-Aldrich).

Cell culture, DNA transfection, and cell synchronization

HeLa cells were cultured in DMEM supplemented with 10% FCS under 5% CO_2 at 37°C as described (Okumoto et al., 2011). CHO cells were cultured in Ham's F-12 medium supplemented with 10% FCS under 5% CO_2 at 37°C as described (Tsukamoto et al., 1990). DNA transfection was performed using Lipofectamine 2000 (Invitrogen) and by electroporation (NEPA21 Super Electroporator; Neppa Gene) as recommended by the manufacturer. Mitotic arrest was performed with 50 ng/ml nocodazole for 12–18 h, and mitotic cells were collected by mitotic shake-off. Adherent cells after shake-off were collected as interphase cells.

LC-MS/MS–based identification of Pex14p phosphorylation sites

Mitotic and interphase HeLa cells were collected by centrifugation at 750 *g* for 5 min. Radioimmunoprecipitation assay

buffer (50 mM Tris-HCl, 0.15 M NaCl, 0.1% wt/vol SDS, 0.5% wt/vol sodium deoxycholate, and 1% wt/vol Nonidet P-40) supplemented with protease inhibitor cocktail complete EDTA-free (Roche) was added to the pellet. After pipetting several times, the cell pellets were lysed on ice for 10 min. After centrifugation at 12,000 *g* for 10 min, the collected supernatants were incubated with antibody to Pex14pN that was immobilized on SureBeads Protein G magnetic beads (Bio-Rad) for 3 h at 4°C with rotation. The beads were washed four times with radioimmunoprecipitation assay buffer and then twice with 50 mM ammonium bicarbonate. Proteins on the beads were digested with 400 ng of trypsin/Lys-C mix (Promega) for 16 h at 37°C. The digests were acidified and desalted using GL-Tip SDS (GL Sciences). The eluates were evaporated and dissolved in 3% acetonitrile (ACN) and 0.1% trifluoroacetic acid.

LC-MS/MS analysis of the resultant peptides was performed on an EASY-nLC 1200 UHPLC connected to a Q Exactive Plus mass spectrometer equipped with a nanoelectrospray ion source (Thermo Fisher Scientific). The peptides were separated on a 75-µm inner diameter × 150 mm C18 reverse-phase column (Nikkyo Technos) with a liner 4–28% ACN gradient for 0–100 min followed by an increase to 80% ACN for 10 min. The mass spectrometer was operated in data-dependent acquisition mode with a top 10 MS/MS method. MS1 spectra were measured with a resolution of 70,000, an automatic gain control target of 10^6, and a mass range from 350 to 1,500 m/z. High-energy collisional dissociation MS/MS spectra were acquired at a resolution of 17,500, an automatic gain control target of 5×10^4, an isolation window of 2.0 m/z, a maximum injection time of 60 ms, and a normalized collision energy of 27. Dynamic exclusion was set to 10 s. Raw data were directly analyzed against the SwissProt database restricted to *Homo sapiens* using Proteome Discoverer v2.3 (Thermo Fisher Scientific) with Mascot search engine v2.5 (Matrix Science) for identification and label-free precursor ion quantification. The search parameters were as follows: (a) trypsin as an enzyme with up to two missed cleavages; (b) precursor mass tolerance of 10 ppm; (c) fragment mass tolerance of 0.02 D; (d) carbamidomethylation of cysteine as a fixed modification; and (e) acetylation of the protein N-terminus, oxidation of methionine, and phosphorylation of serine, threonine, and tyrosine as variable modifications. Peptides were filtered at a false discovery rate of 1% using the percolator node. Normalization was performed such that the total sum of abundance values for each sample over all peptides was the same.

Treatment with λ protein phosphatase and CDK1 inhibitor

Cell lysates and semi-intact cells were treated at 30°C for 30 min with λ protein phosphatase (8 units/µl; New England Biolabs) in phosphatase treatment buffer containing 1 mM $MnCl_2$. For treatment with CDK1 inhibitor, synchronized mitotic HeLa cells were collected, washed with PBS, and cultured for 0–60 min in the presence of 9 µM RO-3306 (Vassilev et al., 2006), CDK1 inhibitor.

siRNA transfection

Knockdown of *CDK1* in HeLa cells was performed by transfection of MISSION siRNA (Sigma-Aldrich) with Lipofectamine 2000, according to the manufacturer's instructions. The sequence of siRNA for human CDK1 was 5′-GGCUUGGAUUUGCUCUCGA(dT)(dT)-3′. MISSION siRNA Universal Negative Control (Sigma-Aldrich) was used as a control.

Generation of *pex14* HeLa cell line using the CRISPR/Cas-9 system

To generate *pex14* HeLa cell line, we used gRNA specific for human *PEX14* (Ran et al., 2013). The target sequence of gRNA was selected using an online CRISPR design tool (MIT, Cambridge, MA). To construct the plasmid coexpressing Cas9 and PEX14gRNA, a pair of oligonucleotides containing the gRNA target sequence was annealed and ligated into the BbsI-linearized pX330 vector (Addgene; Yagita et al., 2017). The pair of oligonucleotides used were 5′-CACCGCTGTAGAAACTTCACTGCCG-3′ and 5′-AAACCGGCAGTGAAGTTTCTACAGC-3′ for *PEX14* gRNA. The resultant plasmid, pX330/PEX14gRNA, was transfected to HeLa cells. Transfected cells were diluted and screened for Pex14p deficiency by immunofluorescence microscopy and immunoblotting. One clonal *pex14* HeLa cell line was used in this study.

DNA construction

A plasmid encoding N-terminally FLAG-tagged rat Pex14p cDNA (Shimizu et al., 1999) was inserted into pcDNA3.1/Zeo (Invitrogen). By using an inverse PCR method (Dominy and Andrews, 2003), the last 45 bp of cytomegalovirus promoter/enhancer region of pcDNA3.1/Zeo was deleted to suppress the overexpression of Pex14p. *PEX14* mutants harboring point mutations were also generated by inverse PCR. To construct plasmids, *PEX14(156–376)* and *PEX14(200-376)*, BglII and XbaI fragments each encoding Pex14p(156–376) and Pex14p(200–376) that were N-terminally fused with FLAG or HA were PCR amplified and ligated into the BamHI/XbaI sites of pcDNA3.1/Zeo.

Morphological analysis

Cells were fixed with 4% PFA, permeabilized with 0.1% Triton X-100 containing 1% BSA (Otera et al., 2002), and incubated with antibodies at RT for 1 h. Rabbit antibodies against PTS1 peptide (Otera et al., 2002), human catalase (Matsumoto et al., 2003), and GFP (Mukai et al., 2019) and guinea pig antibody against Pex14pC (Mukai et al., 2002) were used as primary antibodies. Indirect immunofluorescent staining using secondary antibodies labeled with Alexa Fluor 488 and 568 (Invitrogen) was performed as described (Tamura et al., 2014). Cells were observed on a Zeiss Axioscop with a Plan Apochromat 63× 1.4-NA oil objective lens. In Fig. 3 C, confocal fluorescence microscopy was performed on a Zeiss LSM510 with Axio Observer.Z1 equipped with a Plan Apochromat 100× 1.4-NA oil objective lens and argon plus dual HeNe lasers at RT. Images were acquired with Zen software (Zeiss) and prepared using Photoshop (CS4; Adobe). Peroxisome-restoring activity of the S232 and S334 mutants of Pex14p was verified by counting PTS1- or catalase-positive cells among 100 cells expressing Pex14p and its variants in *pex14* HeLa cells. The import efficiency of WT Pex14p was taken as 100%.

Coimmunoprecipitation assay

HeLa cells were lysed with lysis buffer containing 50 mM Tris-HCl, pH 7.4, 10% glycerol, 0.15 M NaCl, 1% Triton X-100, 1 mM

PMSF, 1 mM EDTA, 1 mM DTT, 25 µg/ml each of antipain and leupeptin, and 50 units of aprotinin (Sigma-Aldrich). Pex14p was immunoprecipitated with rabbit antibody to Pex14pC conjugated to Protein-A-Sepharose (GE Healthcare). *pex14* HeLa cells were transfected with normal or mutant *FLAG-PEX14* and *HA-PEX14*. Cells were directly lysed with the lysis buffer. FLAG-Pex14p and its variants were immunoprecipitated using agarose beads conjugated with anti-FLAG antibody (M2; Sigma-Aldrich). The immunocomplexes were analyzed by SDS-PAGE and immunoblotting.

In vitro peroxisomal Pex5p import and export assays

Assays for import of Pex5p was performed as follows. A PNS fraction was prepared from mitotic and interphase HeLa cells. These cells (5×10^6 each) were homogenized with import buffer containing 0.25 M sucrose, 5 mM Hepes-KOH, pH 7.4, 3 mM $MgCl_2$, 50 mM KCl, and 1 mM DTT. The PNS fraction was obtained by centrifuging the homogenate at 800 *g* for 5 min. Pex5pL was used in peroxisomal import and export assays. Pex5pL cDNA was transcribed and translated using TNT Quick Coupled transcription/translation systems (Promega) with [^{35}S] methionine and [^{35}S]cysteine (Amersham Biosciences) to generate ^{35}S-labeled Pex5pL (Miyata et al., 2009). The import reaction mixture (100 µl) containing [^{35}S]Pex5pL and 5 mg/ml PNS was incubated at 26°C for 1 h. Import of [^{35}S]Pex5pL was verified by its resistance to the treatment with externally added protease in the absence or presence of 1% Triton X-100 as follows. The import reaction mixture was incubated on ice for 30 min with 40 µg/ml proteinase K. After terminating the protease digestion with 1 mM PMSF, the assay mixture was centrifuged at 20,000 *g* for 20 min to separate organelle and cytosolic fractions and analyzed by SDS-PAGE, autoradiography, and immunoblotting. [^{35}S]Pex5pL was detected by a Typhoon FLA 9500 autoimaging analyzer (GE Healthcare).

For Pex5p export reaction, the PNS fraction incubated with [^{35}S]Pex5pL in the import buffer was centrifuged at 20,000 *g* for 20 min to isolate the organelle fraction containing the [^{35}S] Pex5pL-imported peroxisomes. The organelle fraction was resuspended with the cytosolic fraction (1 mg/ml) from mitotic or interphase HeLa cells in export buffer, 5 mM Hepes-KOH, pH 7.4, 3 mM $MgCl_2$, 50 mM KCl, 1 mM DTT, 4% (vol/vol) rabbit reticulocyte lysate, and 3 mM ATP (Miyata et al., 2009). After the export reaction at 26°C for 1 h, the assay mixture was separated into organelle and cytosolic fractions by centrifugation at 20,000 *g* for 20 min. [^{35}S]Pex5pL was detected as above.

Protease digestion assay

PNS fractions were prepared from mitotic and interphase HeLa cells or *pex14* HeLa cells transfected with *PEX14, PEX14S232A*, or *PEX14S232D*. Partial protease-treatment experiments using 0.5 mg/ml of PNS fraction from HeLa cells with 2.5–30 µg/ml proteinase K were performed on ice for 30 min. The digestion was terminated by the addition of 1 mM PMSF. The digests were analyzed by SDS-PAGE and immunoblotting with rabbit antibodies to Pex14pN and Pex14pC.

Other methods

Immunoblotting was performed using electrophoretically transferred samples on polyvinylidene membranes (Bio-Rad) with primary antibodies and secondary antibodies conjugated to HRP (GE Healthsciences; Otera et al., 2002). Antigen–antibody complexes were visualized with an ECL Western blotting detection reagent (GE Healthsciences). BN-PAGE analysis was done using 4–16% Bis-Tris Gel (Invitrogen) as described (Tamura et al., 2014). For Phos-tag PAGE analysis, 50 µM $MnCl_2$ and 25 µM Phos-tag acrylamide (Wako) were added to acrylamide gel before making gel of SDS-PAGE (Kinoshita et al., 2006).

Online supplemental material

Fig. S1 shows that mutation of Ser232 to Ala appeared to induce additional mitotic phosphorylation of rat Pex14p at Ser247. Fig. S2 shows that the import efficiency of a dual mutant Pex14pS232D/S334D was similar to that of S232D, suggesting that S232 is an important phosphorylation site in the regulation of peroxisomal protein import during mitosis. Fig. S3 shows that the specificities of antibodies to Pex14p N- or C-terminal region.

Acknowledgments

We thank Y. Nanri, T. Umemoto, and M. Kawano for technical assistance and the other members of our laboratories for helpful discussion.

This work was supported in part by grants from the Ministry of Education, Culture, Sports, Science and Technology of Japan: Grants-in-Aid for Scientific Research (JP19K06567 to S. Tamura and JP24247038, JP25112518, JP25116717, JP26116007, JP15K14511, JP15K21743, and JP17H03675 to Y. Fujiki); grants from the Takeda Science Foundation (to Y. Fujiki), the Naito Foundation (to Y. Fujiki), the Japan Foundation for Applied Enzymology, and the Novartis Foundation (Japan) for the Promotion of Science (to Y. Fujiki), and Joint Usage and Joint Research Programs of the Institute of Advanced Medical Sciences, University of Tokushima (to Y. Fujiki).

The authors declare no competing financial interests.

Author contributions: K. Yamashita, S. Tamura, M. Honsho, H. Yada, Y. Yagita, and H. Kosako performed experiments. K. Yamashita, S. Tamura, and Y. Fujiki analyzed data. K. Yamashita, S. Tamura, and Y. Fujiki conceived the project and wrote the manuscript with contribution from all authors.

Submitted: 2 January 2020
Revised: 28 April 2020
Accepted: 13 July 2020

References

Barnes, E.A., M. Kong, V. Ollendorff, and D.J. Donoghue. 2001. Patched1 interacts with cyclin B1 to regulate cell cycle progression. *EMBO J.* 20: 2214–2223. https://doi.org/10.1093/emboj/20.9.2214

Barros-Barbosa, A., M.J. Ferreira, T.A. Rodrigues, A.G. Pedrosa, C.P. Grou, M.P. Pinto, M. Fransen, T. Francisco, and J.E. Azevedo. 2019. Membrane topologies of PEX13 and PEX14 provide new insights on the mechanism of protein import into peroxisomes. *FEBS J.* 286:205–222. https://doi.org/10.1111/febs.14697

Dias, A.F., T.A. Rodrigues, A.G. Pedrosa, A. Barros-Barbosa, T. Francisco, and J.E. Azevedo. 2017. The peroxisomal matrix protein translocon is a large cavity-forming protein assembly into which PEX5 protein enters to release its cargo. *J. Biol. Chem.* 292:15287–15300. https://doi.org/10.1074/jbc.M117.805044

Dominy, C.N., and D.W. Andrews. 2003. Site-directed mutagenesis by inverse PCR. *Methods Mol. Biol.* 235:209–223.
Dubreuil, M.M., D.W. Morgens, K. Okumoto, M. Honsho, K. Contrepois, B. Lee-McMullen, G.M. Traber, R.S. Sood, S.J. Dixon, M.P. Snyder, et al. 2020. Systematic identification of regulators of oxidative stress reveals non-canonical roles for peroxisomal import and the pentose phosphate pathway. *Cell Rep.* 30:1417–1433.e7. https://doi.org/10.1016/j.celrep.2020.01.013
Errico, A., K. Deshmukh, Y. Tanaka, A. Pozniakovsky, and T. Hunt. 2010. Identification of substrates for cyclin dependent kinases. *Adv. Enzyme Regul.* 50:375–399. https://doi.org/10.1016/j.advenzreg.2009.12.001
Fodor, K., J. Wolf, K. Reglinski, D.M. Passon, Y. Lou, W. Schliebs, R. Erdmann, and M. Wilmanns. 2015. Ligand-induced compaction of the PEX5 receptor-binding cavity impacts protein import efficiency into peroxisomes. *Traffic.* 16:85–98. https://doi.org/10.1111/tra.12238
Fransen, M., C. Brees, K. Ghys, L. Amery, G.P. Mannaerts, D. Ladant, and P.P. Van Veldhoven. 2002. Analysis of mammalian peroxin interactions using a non-transcription-based bacterial two-hybrid assay. *Mol. Cell. Proteomics.* 1:243–252. https://doi.org/10.1074/mcp.M100025-MCP200
Fujiki, Y.. 1997. Molecular defects in genetic diseases of peroxisomes. *Biochim. Biophys. Acta.* 1361:235–250. https://doi.org/10.1016/S0925-4439(97)00051-3
Fujiki, Y., K. Okumoto, N. Kinoshita, and K. Ghaedi. 2006. Lessons from peroxisome-deficient Chinese hamster ovary (CHO) cell mutants. *Biochim. Biophys. Acta.* 1763:1374–1381. https://doi.org/10.1016/j.bbamcr.2006.09.012
Gatto, G.J., Jr., B.V. Geisbrecht, S.J. Gould, and J.M. Berg. 2000. Peroxisomal targeting signal-1 recognition by the TPR domains of human PEX5. *Nat. Struct. Biol.* 7:1091–1095. https://doi.org/10.1038/81930
Gouveia, A.M., C.P. Guimaraes, M.E. Oliveira, C. Reguenga, C. Sa-Miranda, and J.E. Azevedo. 2003. Characterization of the peroxisomal cycling receptor, Pex5p, using a cell-free in vitro import system. *J. Biol. Chem.* 278:226–232. https://doi.org/10.1074/jbc.M209498200
Harbauer, A.B., M. Opalińska, C. Gerbeth, J.S. Herman, S. Rao, B. Schönfisch, B. Guiard, O. Schmidt, N. Pfanner, and C. Meisinger. 2014. Mitochondria. Cell cycle-dependent regulation of mitochondrial preprotein translocase. *Science.* 346:1109–1113. https://doi.org/10.1126/science.1261253
Hosoi, K.I., N. Miyata, S. Mukai, S. Furuki, K. Okumoto, E.H. Cheng, and Y. Fujiki. 2017. The VDAC2-BAK axis regulates peroxisomal membrane permeability. *J. Cell Biol.* 216:709–722. https://doi.org/10.1083/jcb.201605002
Hunt, T.. 2013. On the regulation of protein phosphatase 2A and its role in controlling entry into and exit from mitosis. *Adv. Biol. Regul.* 53:173–178. https://doi.org/10.1016/j.jbior.2013.04.001
Itoh, R., and Y. Fujiki. 2006. Functional domains and dynamic assembly of the peroxin Pex14p, the entry site of matrix proteins. *J. Biol. Chem.* 281:10196–10205. https://doi.org/10.1074/jbc.M600158200
Johnson, M.A., W.B. Snyder, J.L. Cereghino, M. Veenhuis, S. Subramani, and J.M. Cregg. 2001. *Pichia pastoris* Pex14p, a phosphorylated peroxisomal membrane protein, is part of a PTS-receptor docking complex and interacts with many peroxins. *Yeast.* 18:621–641. https://doi.org/10.1002/yea.711
Kinoshita, E., E. Kinoshita-Kikuta, K. Takiyama, and T. Koike. 2006. Phosphate-binding tag, a new tool to visualize phosphorylated proteins. *Mol. Cell. Proteomics.* 5:749–757. https://doi.org/10.1074/mcp.T500024-MCP200
Knoblach, B., and R.A. Rachubinski. 2010. Phosphorylation-dependent activation of peroxisome proliferator protein PEX11 controls peroxisome abundance. *J. Biol. Chem.* 285:6670–6680. https://doi.org/10.1074/jbc.M109.094805
Lazarow, P.B., and Y. Fujiki. 1985. Biogenesis of peroxisomes. *Annu. Rev. Cell Biol.* 1:489–530. https://doi.org/10.1146/annurev.cb.01.110185.002421
Lazarow, P.B., and H.W. Moser. 1995. Disorders of Peroxisome Biogenesis. *In* The Metabolic Basis of Inherited Disease. Vol. Vol. 7. C.R. Scriver, A.I. Beaudet, W.S. Sly, and D. Valle, editors. McGraw-Hill, New York. pp. 2287–2324.
Matsumoto, N., S. Tamura, and Y. Fujiki. 2003. The pathogenic peroxin Pex26p recruits the Pex1p-Pex6p AAA ATPase complexes to peroxisomes. *Nat. Cell Biol.* 5:454–460. https://doi.org/10.1038/ncb982
Maynard, E.L., G.J.J. Gatto, Jr., and J.M. Berg. 2004. Pex5p binding affinities for canonical and noncanonical PTS1 peptides. *Proteins.* 55:856–861. https://doi.org/10.1002/prot.20112
Meinecke, M., P. Bartsch, and R. Wagner. 2016. Peroxisomal protein import pores. *Biochim. Biophys. Acta.* 1863:821–827. https://doi.org/10.1016/j.bbamcr.2015.10.013
Mindthoff, S., S. Grunau, L.L. Steinfort, W. Girzalsky, J.K. Hiltunen, R. Erdmann, and V.D. Antonenkov. 2016. Peroxisomal Pex11 is a pore-forming protein homologous to TRPM channels. *Biochim. Biophys. Acta.* 1863:271–283. https://doi.org/10.1016/j.bbamcr.2015.11.013
Miyata, N., and Y. Fujiki. 2005. Shuttling mechanism of peroxisome targeting signal type 1 receptor Pex5: ATP-independent import and ATP-dependent export. *Mol. Cell. Biol.* 25:10822–10832. https://doi.org/10.1128/MCB.25.24.10822-10832.2005
Miyata, N., K. Hosoi, S. Mukai, and Y. Fujiki. 2009. In vitro import of peroxisome-targeting signal type 2 (PTS2) receptor Pex7p into peroxisomes. *Biochim. Biophys. Acta.* 1793:860–870. https://doi.org/10.1016/j.bbamcr.2009.02.007
Mukai, S., and Y. Fujiki. 2006. Molecular mechanisms of import of peroxisome-targeting signal type 2 (PTS2) proteins by PTS2 receptor Pex7p and PTS1 receptor Pex5pL. *J. Biol. Chem.* 281:37311–37320. https://doi.org/10.1074/jbc.M607178200
Mukai, S., K. Ghaedi, and Y. Fujiki. 2002. Intracellular localization, function, and dysfunction of the peroxisome-targeting signal type 2 receptor, Pex7p, in mammalian cells. *J. Biol. Chem.* 277:9548–9561. https://doi.org/10.1074/jbc.M108635200
Mukai, S., T. Matsuzaki, and Y. Fujiki. 2019. The cytosolic peroxisome-targeting signal (PTS)-receptors, Pex7p and Pex5pL, are sufficient to transport PTS2 proteins to peroxisomes. *Biochim. Biophys. Acta Mol. Cell Res.* 1866:441–449. https://doi.org/10.1016/j.bbamcr.2018.10.006
Neufeld, C., F.V. Filipp, B. Simon, A. Neuhaus, N. Schüller, C. David, H. Kooshapur, T. Madl, R. Erdmann, W. Schliebs, et al. 2009. Structural basis for competitive interactions of Pex14 with the import receptors Pex5 and Pex19. *EMBO J.* 28:745–754. https://doi.org/10.1038/emboj.2009.7
Oeljeklaus, S., A. Schummer, T. Mastalski, H.W. Platta, and B. Warscheid. 2016. Regulation of peroxisome dynamics by phosphorylation. *Biochim. Biophys. Acta.* 1863:1027–1037. https://doi.org/10.1016/j.bbamcr.2015.12.022
Okumoto, K., S. Misono, N. Miyata, Y. Matsumoto, S. Mukai, and Y. Fujiki. 2011. Cysteine ubiquitination of PTS1 receptor Pex5p regulates Pex5p recycling. *Traffic.* 12:1067–1083. https://doi.org/10.1111/j.1600-0854.2011.01217.x
Oliveira, M.E.M., C. Reguenga, A.M.M. Gouveia, C.P. Guimarães, W. Schliebs, W.-H. Kunau, M.T. Silva, C. Sá-Miranda, and J.E. Azevedo. 2002. Mammalian Pex14p: membrane topology and characterisation of the Pex14p-Pex14p interaction. *Biochim. Biophys. Acta.* 1567:13–22. https://doi.org/10.1016/S0005-2736(02)00635-1
Olsen, J.V., M. Vermeulen, A. Santamaria, C. Kumar, M.L. Miller, L.J. Jensen, F. Gnad, J. Cox, T.S. Jensen, E.A. Nigg, et al. 2010. Quantitative phosphoproteomics reveals widespread full phosphorylation site occupancy during mitosis. *Sci. Signal.* 3:ra3. https://doi.org/10.1126/scisignal.2000475
Otera, H., T. Harano, M. Honsho, K. Ghaedi, S. Mukai, A. Tanaka, A. Kawai, N. Shimizu, and Y. Fujiki. 2000. The mammalian peroxin Pex5pL, the longer isoform of the mobile peroxisome targeting signal (PTS) type 1 transporter, translocates the Pex7p.PTS2 protein complex into peroxisomes via its initial docking site, Pex14p. *J. Biol. Chem.* 275:21703–21714. https://doi.org/10.1074/jbc.M000720200
Otera, H., K. Setoguchi, M. Hamasaki, T. Kumashiro, N. Shimizu, and Y. Fujiki. 2002. Peroxisomal targeting signal receptor Pex5p interacts with cargoes and import machinery components in a spatiotemporally differentiated manner: conserved Pex5p WXXXF/Y motifs are critical for matrix protein import. *Mol. Cell. Biol.* 22:1639–1655. https://doi.org/10.1128/MCB.22.6.1639-1655.2002
Pedrosa, A.G., T. Francisco, D. Bicho, A.F. Dias, A. Barros-Barbosa, V. Hagmann, G. Dodt, T.A. Rodrigues, and J.E. Azevedo. 2018. Peroxisomal monoubiquitinated PEX5 interacts with the AAA ATPases PEX1 and PEX6 and is unfolded during its dislocation into the cytosol. *J. Biol. Chem.* 293:11553–11563. https://doi.org/10.1074/jbc.RA118.003669
Platta, H.W., and R. Erdmann. 2007. Peroxisomal dynamics. *Trends Cell Biol.* 17:474–484. https://doi.org/10.1016/j.tcb.2007.06.009
Platta, H.W., R. Brinkmeier, C. Reidick, S. Galiani, M.P. Clausen, and C. Eggeling. 2016. Regulation of peroxisomal matrix protein import by ubiquitination. *Biochim. Biophys. Acta.* 1863:838–849. https://doi.org/10.1016/j.bbamcr.2015.09.010
Platta, H.W., S. Grunau, K. Rosenkranz, W. Girzalsky, and R. Erdmann. 2005. Functional role of the AAA peroxins in dislocation of the cycling PTS1 receptor back to the cytosol. *Nat. Cell Biol.* 7:817–822. https://doi.org/10.1038/ncb1281
Ran, F.A., P.D. Hsu, J. Wright, V. Agarwala, D.A. Scott, and F. Zhang. 2013. Genome engineering using the CRISPR-Cas9 system. *Nat. Protoc.* 8:2281–2308. https://doi.org/10.1038/nprot.2013.143

Reguenga, C., M.E.M. Oliveira, A.M.M. Gouveia, C. Sá-Miranda, and J.E. Azevedo. 2001. Characterization of the mammalian peroxisomal import machinery: Pex2p, Pex5p, Pex12p, and Pex14p are subunits of the same protein assembly. *J. Biol. Chem.* 276:29935–29942. https://doi.org/10.1074/jbc.M104114200

Salazar-Roa, M., and M. Malumbres. 2017. Fueling the Cell Division Cycle. *Trends Cell Biol.* 27:69–81. https://doi.org/10.1016/j.tcb.2016.08.009

Schwerter, D., I. Grimm, W. Girzalsky, and R. Erdmann. 2018. Receptor recognition by the peroxisomal AAA complex depends on the presence of the ubiquitin moiety and is mediated by Pex1p. *J. Biol. Chem.* 293:15458–15470. https://doi.org/10.1074/jbc.RA118.003936

Shimizu, N., R. Itoh, Y. Hirono, H. Otera, K. Ghaedi, K. Tateishi, S. Tamura, K. Okumoto, T. Harano, S. Mukai, et al. 1999. The peroxin Pex14p. cDNA cloning by functional complementation on a Chinese hamster ovary cell mutant, characterization, and functional analysis. *J. Biol. Chem.* 274:12593–12604. https://doi.org/10.1074/jbc.274.18.12593

Shiota, T., A. Traven, and T. Lithgow. 2015. Mitochondrial biogenesis: cell-cycle-dependent investment in making mitochondria. *Curr. Biol.* 25:R78–R80. https://doi.org/10.1016/j.cub.2014.12.006

Smoyer, C.J., and S.L. Jaspersen. 2014. Breaking down the wall: the nuclear envelope during mitosis. *Curr. Opin. Cell Biol.* 26:1–9. https://doi.org/10.1016/j.ceb.2013.08.002

Su, J.R., K. Takeda, S. Tamura, Y. Fujiki, and K. Miki. 2009. Crystal structure of the conserved N-terminal domain of the peroxisomal matrix protein import receptor, Pex14p. *Proc. Natl. Acad. Sci. USA.* 106:417–421. https://doi.org/10.1073/pnas.0808681106

Taguchi, N., N. Ishihara, A. Jofuku, T. Oka, and K. Mihara. 2007. Mitotic phosphorylation of dynamin-related GTPase Drp1 participates in mitochondrial fission. *J. Biol. Chem.* 282:11521–11529. https://doi.org/10.1074/jbc.M607279200

Tamura, S., N. Matsumoto, R. Takeba, and Y. Fujiki. 2014. AAA peroxins and their recruiter Pex26p modulate the interactions of peroxins involved in peroxisomal protein import. *J. Biol. Chem.* 289:24336–24346. https://doi.org/10.1074/jbc.M114.588038

Tamura, S., N. Shimozawa, Y. Suzuki, T. Tsukamoto, T. Osumi, and Y. Fujiki. 1998. A cytoplasmic AAA family peroxin, Pex1p, interacts with Pex6p. *Biochem. Biophys. Res. Commun.* 245:883–886. https://doi.org/10.1006/bbrc.1998.8522

Tanaka, K., M. Soeda, Y. Hashimoto, S. Takenaka, and M. Komori. 2012. Identification of phosphorylation sites in *Hansenula polymorpha* Pex14p by mass spectrometry. *FEBS Open Bio.* 3:6–10. https://doi.org/10.1016/j.fob.2012.11.001

Tsukamoto, T., S. Yokota, and Y. Fujiki. 1990. Isolation and characterization of Chinese hamster ovary cell mutants defective in assembly of peroxisomes. *J. Cell Biol.* 110:651–660. https://doi.org/10.1083/jcb.110.3.651

Uchiyama, K., E. Jokitalo, M. Lindman, M. Jackman, F. Kano, M. Murata, X. Zhang, and H. Kondo. 2003. The localization and phosphorylation of p47 are important for Golgi disassembly-assembly during the cell cycle. *J. Cell Biol.* 161:1067–1079. https://doi.org/10.1083/jcb.200303048

Vassilev, L.T., C. Tovar, S. Chen, D. Knezevic, X. Zhao, H. Sun, D.C. Heimbrook, and L. Chen. 2006. Selective small-molecule inhibitor reveals critical mitotic functions of human CDK1. *Proc. Natl. Acad. Sci. USA.* 103:10660–10665. https://doi.org/10.1073/pnas.0600447103

Wang, Z., M. Fan, D. Candas, T.Q. Zhang, L. Qin, A. Eldridge, S. Wachsmann-Hogiu, K.M. Ahmed, B.A. Chromy, D. Nantajit, et al. 2014. Cyclin B1/Cdk1 coordinates mitochondrial respiration for cell-cycle G2/M progression. *Dev. Cell.* 29:217–232. https://doi.org/10.1016/j.devcel.2014.03.012

Wu, J.Q., J.Y. Guo, W. Tang, C.S. Yang, C.D. Freel, C. Chen, A.C. Nairn, and S. Kornbluth. 2009. PP1-mediated dephosphorylation of phosphoproteins at mitotic exit is controlled by inhibitor-1 and PP1 phosphorylation. *Nat. Cell Biol.* 11:644–651. https://doi.org/10.1038/ncb1871

Yagita, Y., K. Shinohara, Y. Abe, K. Nakagawa, M. Al-Owain, F.S. Alkuraya, and Y. Fujiki. 2017. Deficiency of a retinal dystrophy protein, acyl-CoA binding domain-containing 5 (ACBD5), impairs peroxisomal β-oxidation of very-long-chain fatty acids. *J. Biol. Chem.* 292:691–705. https://doi.org/10.1074/jbc.M116.760090

Yeong, F.M.. 2013. Multi-step down-regulation of the secretory pathway in mitosis: a fresh perspective on protein trafficking. *BioEssays.* 35:462–471. https://doi.org/10.1002/bies.201200144

Supplemental material

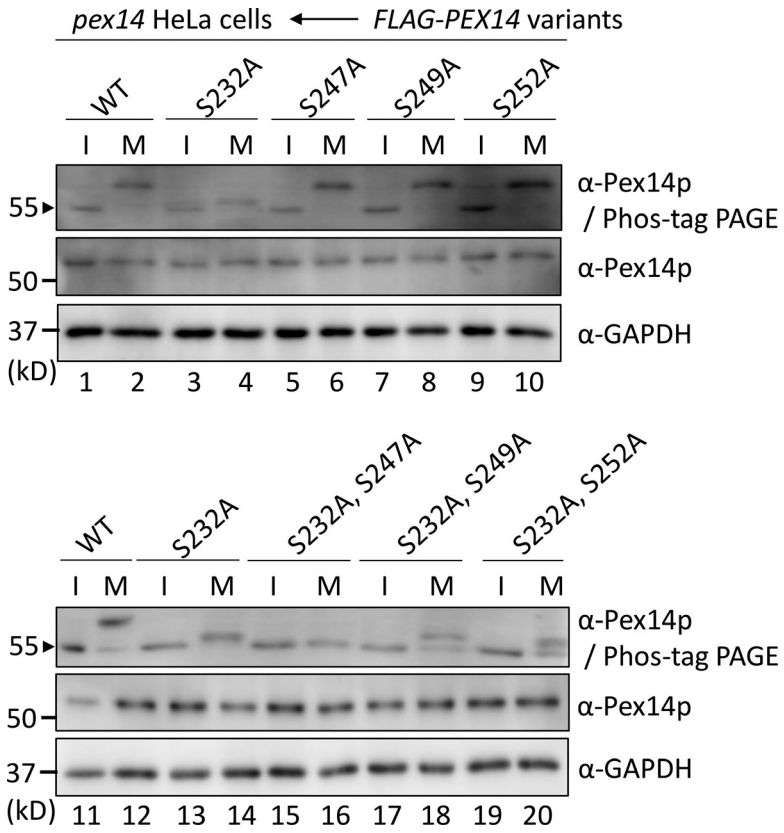

Figure S1. **Phos-tag PAGE analysis of WT Pex14p and its mutants.** Four potential phosphorylation sites of Pex14p were substituted to Ala, two of which are shown in Fig. 2 E (upper panels). Pex14p mutants with two-site mutations were likewise analyzed (lower panels). M, mitotic-phase cells; I, interphase cells.

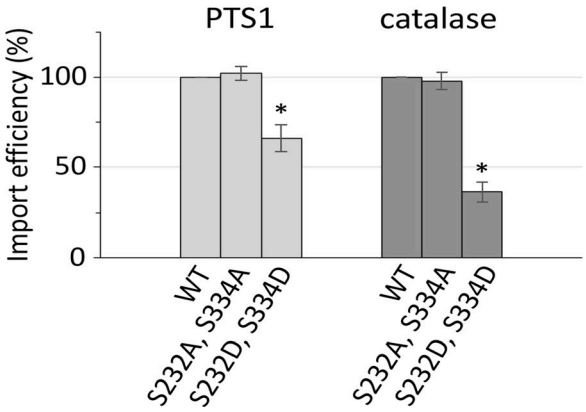

Figure S2. **Phosphomimetic Pex14p suppresses peroxisomal import of matrix proteins.** Pex14p variants mutated at both S232 and S334 were assessed for peroxisomal protein import in *pex14* HeLa cells as in Fig. 3 (A and B). Error bars show SEM. Statistical significance was verified by ANOVA and post hoc Dunnett's test, and the significance is indicated with asterisk (*, $P < 0.001$, $n = 4$).

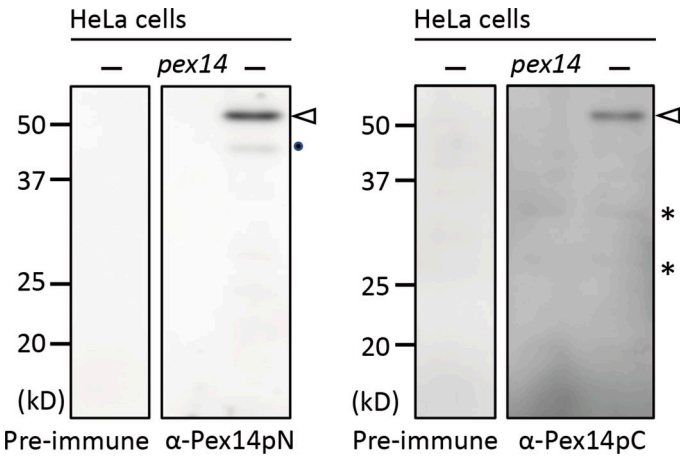

Figure S3. **PNS fractions from control HeLa (–) and *pex14* HeLa cells were analyzed by SDS-PAGE and immunoblotting with antibodies to Pex14pN (left) and Pex14pC (right).** Open arrowheads indicate the endogenous Pex14p. The dot designates a cleaved product of Pex14p; *, nonspecific bands.